ELSEVIER

23 August 1996

Chemical Physics Letters 258 (1996) 644–650

CHEMICAL PHYSICS LETTERS

Vibronic interactions in NO_3: from the $^2E'$ origin region to the $NO + O_2$ reactive channel

L. Valachovic, C. Riehn [1], K. Mikhaylichenko, C. Wittig

Department of Chemistry, University of Southern California, Los Angeles, CA 90089-0482 USA

Received 28 February 1996; in final form 18 June 1996

Abstract

LIF spectra of expansion-cooled NO_3 in the region 595–666 nm reveal vibronic interactions responsible for $^2E'$ radiationless decay. A hierarchy of coupling strengths is suggested. Due the large atomic masses, tunneling results in small unimolecular decomposition rates below the $NO + O_2$ barrier on the $^2A'_2$ ground potential surface. These have been observed via their quenching of long-lived NO_3 fluorescence, and rates as small as 3×10^4 s^{-1} are reported. This is 5 orders of magnitude smaller than the rate just above the barrier, which had been determined previously by using the ultrafast pump–probe technique.

1. Introduction

Although the gaseous nitrate radical, NO_3, was first observed spectroscopically well over a century ago [1], its photophysics and photochemistry continue to provide many experimental and theoretical challenges and surprises. It possesses strong absorption features which span the visible and near-infrared portions of the spectrum, making it an ideal candidate for studies of photoinduced processes. Moreover, these spectral features have been measured with high precision at temperatures down to 200 K because of NO_3's importance in the upper atmosphere as a powerful oxidizing agent during the night [2]. Despite numerous spectroscopic and kinetics studies [3], the intramolecular and dissociation dynamics of NO_3 are still not understood in detail, even though it has an attractive energy level structure for examining a number of chemical and physical processes both one at a time and in competition with one another (see Fig. 1). Specifically, because of the unique proximities of the reactive channels, the qualitatively different transition states (i.e., tight versus loose), and the different possibilities for accessing decay routes, NO_3 is well suited as a prototype for detailed studies of unimolecular decomposition. The reason it has not received more attention is experimental, namely, the difficulty of preparing clean, well-characterized samples at suitable concentrations.

The three lowest electronic states of NO_3 (the $^2A'_2$ ground state, $^2E''$ at 7005 cm^{-1}, and $^2E'$ at 15110

[1] Address: Universität Frankfurt am Main, Institut für Physikalische und Theoretische Chemie, Marie-Curie-Str. 11, D-60439 Frankfurt am Main, Germany.

PII S0009-2614(96)00703-8

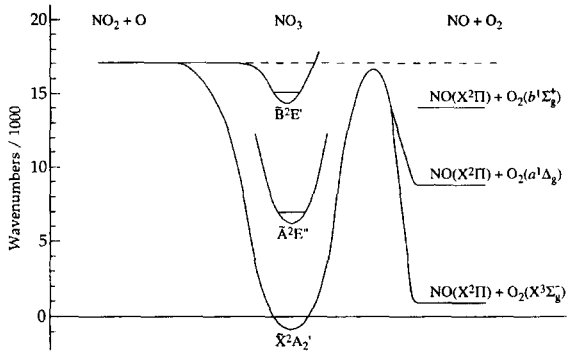

Fig. 1. Diagram showing low-lying NO_3 electronic states and dissociation channels.

cm^{-1}) are subject to strong vibronic interactions such as Jahn–Teller (JT) and pseudo-Jahn–Teller (PJT) [3–5]. Cederbaum and coworkers have carried out comprehensive analyses [6] of the 266 nm NO_3^- photoelectron spectra recorded by Weaver et al. [3]. By fitting eigenvalues of the NO_3 electronic Hamiltonian to calculated (ab initio) ionization potentials of the anion, they determined the values of the diabatic electronic matrix elements necessary for simulating those portions of the photoelectron spectra dominated by the $^2A'_2$ state. Their results confirmed the prominent role played by $^2A'_2/^2E'$ PJT coupling in the intramolecular dynamics. Both mode-mode couplings between the degenerate vibrations and couplings via the symmetric mode were shown to contribute significantly. Matrix elements between $^2E''$ and $^2A'_2$ were deemed to be of minor importance in calculating the $^2A'_2$ portions of the photoelectron spectra since they involve nuclear displacements of order bilinear or higher. They were also able to explain why the NO_3 ground state appears to be D_{3h}, despite evidence for a C_{2v} minimum resulting from PJT interaction. Namely, though PJT interaction between $^2A'_2$ and $^2E'$ leads to shallow minima at 3 equivalent C_{2v} positions, vibrational averaging results in an effective D_{3h} structure.

The photoelectron spectrum at 213 nm recorded by Weaver et al. includes features of the $^2E''$ state, which also displays vibronic interactions. However, the respective roles of interstate PJT coupling ($^2E''$ with $^2A'_2$ and/or $^2E'$) and intrastate JT coupling remain unknown. This knowledge is important since $^2E''/^2E'$ vibronic couplings may be pertinent to NO_3 spectra such as those reported here.

Photoexcitation of internally cold NO_3 at wavelengths shorter than 595 nm results in unimolecular decomposition under collision-free conditions, with the $NO + O_2$ channel dominating down to 585.8 nm and the $NO_2 + O$ channel dominating at larger photon energies.

$$NO_3 \xrightarrow{k_1} NO + O_2 \quad (1)$$

$$NO_3 \xrightarrow{k_2} O + NO_2 \quad (2)$$

Reaction (1) involves a tight transition state with significant nuclear and electronic rearrangements, and since tunneling occurs at energies below the top of the barrier, there can be no precise threshold. Rather, the collision-free dissociation rate, $k_1(E)$, drops very rapidly as the energy is tuned to successively lower values below the top of the barrier. Note that although tunneling probabilities are quite small for heavier masses (i.e., relative to hydrogen), tunneling will nonetheless dominate as long as the rates for competitive decay processes are smaller. Indeed, this is the case here since the NO_3 fluorescence decay rates are significantly smaller than the smallest tunneling rates which were measured.

On the basis of measurements of product translational energy distributions, the O_2 product is known to be formed with considerable internal excitation [7,8]. Namely, there is a marked population inversion, with the O_2 internal distribution peaking near 10000 cm^{-1}.

NO_3 fluorescence is observed at excitation wavelengths longer than ≈ 593 nm. It is clear that the $^2E' \leftarrow {}^2A'_2$ oscillator strength is shared between the zeroth-order $^2E'$ level and otherwise nonradiative levels belonging to the $^2A'_2$ and/or $^2E''$ manifolds. Specifically, though the peak absorption cross section at 662 nm is large ($\sigma = 2.2 \times 10^{-17}$ cm^2 at 298 K [9] [2]), fluorescence lifetimes have been shown to exceed 100 μs [5]. It is this large dilution of the

[2] Since the parameter σ was obtained by using the expression $I = I_0 \exp\{-\sigma N x\}$, where N is the total NO_3 density, the cross section per quantum state is much larger, indicating an exceptionally strong absorber.

oscillator strength that implicates the lower zeroth-order surfaces. Thus, NO_3 displays the Douglas effect [10], and its photophysics can be understood within the framework of radiationless transition theory [3,4,11–13].

Nonadiabatic couplings in this system strongly influence the short time dynamics, though any propensity for such couplings to involve vibrational selection rules must be viewed within the framework of intramolecular vibrational redistribution (IVR). For example, 'modes' accessed via vibronic interaction will decay into bath states on a time scale dictated by IVR. The corresponding spectral widths are expected to be narrower than those of $^2E'$ radiationless decay, which occurs in only ≈ 100 fs (vide infra). Weaker interactions such as second-order spin–orbit, orbit–rotation, etc. have matrix elements which are typically tenths of wavenumbers, corresponding to rates which are also faster than the known values of k_1 [11]. Thus, on the long timescale of reaction (1), the system is expected to be quantum ergodic, manifesting vibronic and even rovibronic chaos. Such a hierarchy of coupling strengths can provide observables that offer insight into the dynamics.

In this Letter, we report NO_3 LIF spectra obtained with samples that have been expansion-cooled to $T_{rot} \approx 6$ K by using a heated, pulsed nozzle of the Chen design [14] to thermally decompose an N_2O_5 precursor. This has enabled us to record good S/N spectra that display the large number of transitions characteristic of vibronic interactions. Though high resolution spectra are fundamentally unassignable due to the chaotic character of the nuclear dynamics, the multimode nature of the vibrational dynamics is evidenced in the region of the $^2E'$ origin by the presence of about a dozen 'clumps' having widths and spacings each of ≈ 10 cm^{-1}. PJT interaction is known to couple $^2A'_2$ and $^2E'$ [3–5], and it is possible that coupling between $^2E'$ and $^2E''$ may also be active. Above the $^2E'$ origin, spectral congestion increases until, at energies where reaction (1) starts to occur, the LIF spectrum is effectively continuous (at least for ≈ 6 K samples). As mentioned above, tunneling below the barrier of reaction (1) leads to very small dissociation rates. By monitoring the time-resolved fluorescence, these collision-free decomposition rates have been determined via their quenching of the long-lived fluorescence, and rates as small as 3×10^4 s^{-1} are reported.

2. Experiment and results

An intense source of internally cold NO_3 radicals was generated by expanding pyrolyzed N_2O_5 in a pulsed jet. N_2O_5 samples were prepared by reaction of NO_2 with O_3 [15], stored at 196 K, and warmed to 260 K for experiments. The radical source consists of a SiC tube (21 mm $\times$ 2.2 mm od $\times$ 1.2 mm id) attached to the output of a 10 Hz pulsed nozzle, as shown in Fig. 2. The SiC tube was resistively heated between two brass electrodes as a mixture of 2% N_2O_5 in Ar, at a total pressure of 1.1 atm, was expanded through the heated region into the vacuum chamber. A water-cooled block was mounted between the nozzle and the SiC tube to prevent thermal decomposition of N_2O_5 prior to expansion. The NO_3 concentration was optimized by varying temperature and pressure to maximize the LIF signal at the $^2E' \leftarrow {}^2A'_2$ origin. NO_2 is a product of N_2O_5 decomposition and displays LIF spectra in the same spectral region as does NO_3. However, its contribution to the LIF spectrum is minor since the NO_2 integrated absorption coefficient is approximately two orders of magnitude smaller than that of NO_3 in this wavelength region. Contributions from NO_2 background only become significant after extensive nozzle usage; they can be minimized by cleaning the nozzle at frequent intervals. LIF signals from N_2O_5 are unlikely since it does not absorb in the visible [16].

The nozzle used here is the best pulsed source of cold NO_3 reported to date. More than 90% of the expanded NO_3 populated $v = 0$, as indicated by the

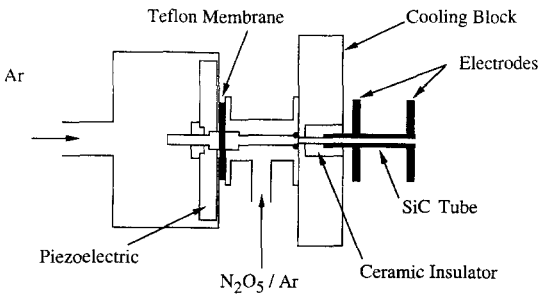

Fig. 2. Schematic diagram of the pulsed pyrolysis nozzle.

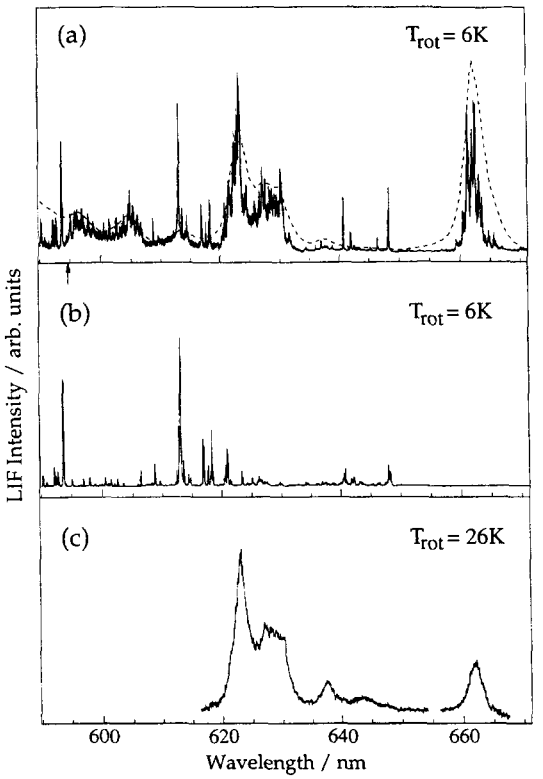

Fig. 3. (a) LIF spectrum of NO_3, including contaminant NO_2 lines; $T_{rot} = 6$ K for coexpanded NO_2; the dashed line is the 230 K absorption spectrum [20]. (b) NO_2 LIF spectrum for $T_{rot} = 6$ K. (c) Same as (a), but $T_{rot} = 26$ K; the 662 nm band is not normalized relative to the other bands (note the break in the spectrum).

absence of hot bands at 678.1 and 637.2 nm [17], as shown in Fig. 3. The NO_3 rotational temperature was assumed to be comparable to that of the coexpanded NO_2. T_{rot} for NO_2 was determined via LIF spectra of the rotational transitions near 593.4 nm by comparing the relative intensities of the $R(0)/R(2)$ and $P(2)/P(4)$ lines to spectra recorded at ≈ 3 K [18]. At a distance of ≈ 22 mm from the nozzle (i.e., in the region where NO_3 was probed), T_{rot} for NO_2 was found to be 6 K. Probing NO_2 further downstream yielded similar rotational temperatures.

The output from a Nd:YAG-pumped dye laser system (Quanta-Ray, DCR-1A/ PDL-1; 0.35 cm^{-1} linewidth), intersected the molecular beam perpendicular to the expansion axis. Fluorescence was collected perpendicular to the laser/molecular beam plane with a PMT which monitored a 3 mm region along the central portion of the nozzle expansion. Higher resolution scans of the $^2E'$ origin were recorded by using an excimer pumped dye laser system (Lumonics TE-840 (XeCl); Lambda Physik FL3002; 0.07 cm^{-1} linewidth with an intracavity etalon).

An LIF spectrum for the region 590-671 nm is shown in Fig. 3a. Spectral features are in accord with the 230 K absorption spectrum [19]. The rapid fall-off of the LIF signal below 594.6 nm is due to opening of the $NO + O_2$ dissociation channel. Since background NO_2 is present, its 6 K spectrum is shown in Fig. 3b. All NO_3 features show less congestion than previously reported [17,20–22]. Spectral congestion is strongly dependent on the degree of rotational cooling, as seen by comparing Figs. 3a and 3c. Note that the overall widths of the vibronic bands do not change upon reducing the rotational temperature from 26 to 6 K. Such behavior is typical for excitation to mixed electronic manifolds. It is difficult to assign vibrational quanta to the observed bands due to the effects of multimode vibronic coupling on the shallow $^2E'$ surface [12]. At these energies, JT and PJT interactions can greatly affect the potential surfaces, and only the (0000) and (1000) vibrational levels (centered at 662 and 623 nm, respectively) can be assigned with any confidence.

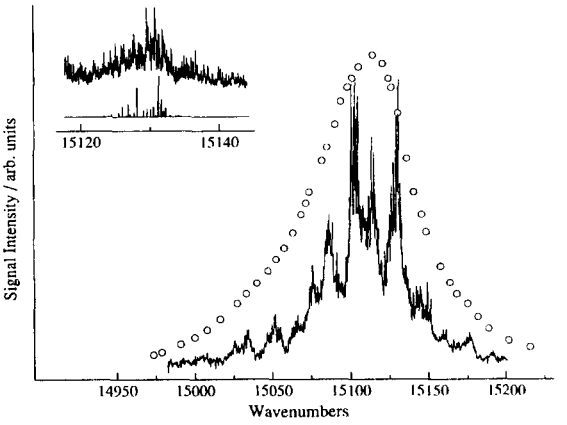

Fig. 4. LIF spectrum of the NO_3 origin region; included is the 220 K absorption spectrum of Ref. [9] (circles). Fitting to a Lorentzian lineshape gives 50 cm^{-1} FWHM. The large number of transitions, even at $T_{rot} = 6$ K, can be seen in the 0.07 cm^{-1} resolution scan shown in the inset; a 6 K simulation (lower entry) shows far fewer lines.

The LIF spectrum of the $^2E' \leftarrow {}^2A'_2$ origin region is shown in Fig. 4. Approximately 12 substructures, each of $\approx 10\ cm^{-1}$ FWHM, extend over $150\ cm^{-1}$. The spectra are highly congested and unassignable, and the full spectral width cannot be accounted for by the NO_3 rotational population, as was correctly deduced by Nelson et al. [5]. Instead, each substructure width corresponds approximately to the calculated rotational width. For comparison, a portion of the spectrum taken at higher resolution is shown in the inset of Fig. 4 along with a simulation of the excitation spectrum for a D_{3h} oblate top. The $^2A'_2$ ground state rotational constants were obtained from Ishiwata et al. [23]. The $^2E'$ rotational constants were calculated ab initio [24] and correspond to an N-O bond length of 1.376 Å.

At wavelengths shorter than 596 nm, it was possible to observe quenching of NO_3 fluorescence via reaction (1). For these measurements, the PMT was placed on the expansion axis 30 cm from the interaction region in order to obtain the slowest possible signal decay curves. A Schott RG695 filter was used to block scattered laser light, and NO_3 was probed at photon energies where contributions to the signals from NO_2 are insignificant. As the wavelength was lowered below 595.5 nm, the time-resolved fluorescence traces displayed the opening of reactive channels, as shown in Fig. 5. Reaction rates can be derived from these traces, and a preliminary analysis indicates that the rate changes by 3 orders of magnitude over an interval of only $100\ cm^{-1}$. Since the $k(E)$ slope did not change when the average chamber pressure (during nozzle operation) was reduced by a factor of ten (to 8×10^{-6} Torr), we believe these measurements reflect collision-free rates. Unfortunately, to achieve the lower chamber pressure, the nozzle stagnation pressure was decreased, resulting in a warmer expansion and higher rates at a given photolysis wavelength (not shown). Though collision-free rates as small as $2 \times 10^4\ s^{-1}$ were obtained under optimum conditions, even smaller rates could be obtained by lowering the background pressure, since beam-gas collisions quench the long-lived mixed $^2E'/{}^2A'_2$ levels. The slow collision-free rates shown in Fig. 5 are attributed to tunneling, which is expected to display a pronounced energy dependence because of the large effective mass in this system.

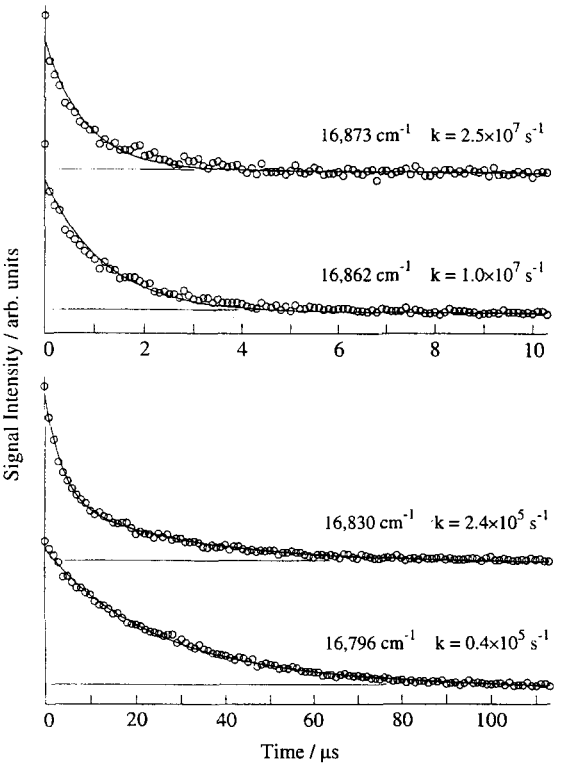

Fig. 5. Time resolved NO_3 emission for the indicated photon energies. Temporal shapes reflect fluorescence depletion as well as the apparatus function. Rates are extracted by using biexponential fits.

For measurements of such slow rates, the fluorescence depletion technique is much more reliable than monitoring NO buildup via pump–probe methods, since nascent product velocities efficiently transport the NO out of the observation region in ≈ 1 μs. Thus, the present approach provides a convenient means of probing tunneling and other weak couplings to continua that would be exceedingly difficult to measure in the frequency domain.

3. Discussion

The present results indicate that radiationless decay of the zeroth-order $^2E'$ electronic state is facile. The spectral width of the origin band at 662 nm corresponds to a $^2E'$ lifetime of ≈ 100 fs, and it is reasonable to assume that at higher energies the $^2E'$ lifetimes are at least as short.

The fact that the LIF spectrum shown in Fig. 4 displays clump-like features raises the question of whether one can speak of vibrational quantum numbers within the lower manifolds at these energies. Specifically, in the coupling between $^2E'(0000)$ and near isoenergetic vibrational levels within the $^2A'_2$ and possibly $^2E''$ manifolds, do vibrations within the lower manifolds obey selection rules for promoting modes? If so, the corresponding quantum numbers will only be valid for short times since they will be destroyed by IVR. Extensive couplings are indicated by the spectra recorded at higher resolution, where the observed density of lines greatly exceeds that which can be attributed to 6 K rotational excitation for a pure $^2E' \leftarrow {}^2A'_2$ band. Hence, one rationalization of the experimental observations is a hierarchy in which vibronic coupling between the zeroth-order electronic states produces the 50 cm^{-1} width of the band shown in Fig. 4, with the lumpiness reflecting a tendency to obey vibrational selection rules. These vibronically mixed levels then decay via IVR, as reflected by the widths of individual clumps. This model differs from the earlier suggestion [5] that $^2E'$ radiationless decay occurs via matrix elements having comparable magnitudes over the entire range of the interaction, which would instead yield a smooth Lorentzian profile for the 662 nm spectral feature [25].

Molecular properties relevant to this system include vibrational level densities within the $^2A'_2$ and $^2E''$ manifolds and matrix elements that couple $^2E'(0000)$ to nearby $^2A'_2$ and $^2E''$ vibrational levels. Several ad hoc coupling schemes were considered as possible rationalizations of the origin-region spectrum. For example, by invoking $^2E'/{}^2A'_2$ selection rules (e.g., $\Delta v_{3(4)} = 1$) and a harmonic oscillator approximation, it was possible to obtain $^2A'_2$ spacings having the same order of magnitude as the clumps shown in Fig. 4 (i.e., a mean spacing of ≈ 2.5 cm^{-1} was calculated for a 160 cm^{-1} interval centered at 15100 cm^{-1} by using $\Delta v_4 = 1$ [3]). Thus, short-lived quantum numbers ascribed to promoting modes may play a role in the dynamics. Coupling between $^2E'$ and $^2E''$ may be weak since bilinear coupling is required (i.e., odd quanta of $\nu_2(a''_2)$ plus one of the e′ modes). However, we leave open the possibility of $^2E''$ participation. Though matrix elements for transitions involving single quantum changes in the ν_3 and ν_4 modes at much lower energies have been shown to be substantial for $^2E'/{}^2A'_2$ coupling (2840 and 1325 cm^{-1} respectively [6]), the matrix elements between $^2E'(0000)$ and near-isoenergetic vibrational levels within $^2E''$ and/or $^2A'_2$ are expected to be small because of poor overlap between the vibrational wavefunctions.

Estimating coupling matrix elements at these energies is difficult because (i) the magnitudes of JT interactions within $^2E'$ and $^2E''$ are unknown, (ii) JT and PJT interactions cannot be treated separately, and (iii) multimode coupling effects are unknown. Clearly, a unique mechanism cannot be determined at this time.

The spectra are of insufficient resolution to overcome the congestion inherent to 6 K NO_3 samples; rather, they serve to display qualitative features. However, since vibronic interactions efficiently promote chaotic nuclear dynamics, high-resolution spectra are expected to be fundamentally unassignable. In this case the underlying physics can only be revealed through statistical analyses, and even here it is necessary to obtain pure sequences (e.g., fixed values of total angular momentum) before applying statistical methods.

When photon energies are increased sufficiently, unimolecular reactions commence. This first occurs below the barrier on the $^2A'_2$ surface. By monitoring time-resolved NO_3 LIF under conditions where reaction (1) quenches this emission, it has been possible to measure rates as small as 3×10^4 s^{-1} which correspond to energies ≈ 100 cm^{-1} below the barrier (see Fig. 5). This is 5 orders of magnitude smaller than the rates obtained at higher energies by using the picosecond-resolution pump–probe technique [11], from which it was concluded that the rate just above the barrier is $\approx 10^9$ s^{-1}. The very small rates reported here can be attributed to tunneling below the barrier, namely, the rates can be fitted by using a one-dimensional model. Preliminary analyses have fitted the $k(E)$ data by assuming a threshold RRKM rate of 10^9 s^{-1} and multiplying this by the tunneling probability, which was calculated by using a modified WKB approximation [26,27] with a re-

[3] This mean spacing retains e′ vibrational degeneracy.

duced mass of 8 amu and a parabolic barrier having a ≈ 1 Å width 100 cm^{-1} below its maximum.

Since vibronic coupling is very efficient, it seems unlikely that the $O + NO_2$ channel is accessed only via the zeroth-order $^2E'$ surface. If this were the case, the mechanism would be unimolecular decay on a potential surface bound by ≈ 1700 cm^{-1}. Though this would occur rapidly, it would not occur so rapidly as to completely bypass the efficient radiationless decay channel. Thus, in accordance with the suggestion by Davis et al. [7], we believe that the $^2A'_2$ and possibly $^2E''$ zeroth-order surfaces also participate in reaction (2). Determining the magnitudes of the linear and bilinear vibronic couplings, though daunting, will be important for understanding the detailed reaction mechanism.

Acknowledgements

The authors benefited from discussions with D.W. Arnold, H. Reisler, P.I. Ionov, A. Sanov, R.A. Beaudet, and H.F. Davis. This research was supported by the US Department of Energy.

References

[1] P. Hautefeuille and J. Chappuis, CR Acad. Sci. Paris 92 (1881) 80.
[2] R.P. Wayne, I. Barnes, P. Biggs, J.P. Burrows, C.E. Canosa-Mas, J. Hjorth, G. LeBras, G.K. Moortgat, D. Perner, G. Poulet, G. Restelli and H. Sidebottom, in: The nitrate radical: physics, chemistry, and the atmosphere, Atmospheric Environment 25A, ed. R.P. Wayne (Pergamon Press, Oxford, 1991) pp. 1-206.
[3] A. Weaver, D.W. Arnold, S.E. Bradforth and D.M. Neumark, J. Chem. Phys. 94 (1991) 1740, and references therein.
[4] E. Hirota, K. Kawaguchi, T. Ishiwata and I. Tanaka, J. Chem. Phys. 95 (1991) 771.
[5] H.H. Nelson, L. Pasternack and J.R. McDonald, J. Chem. Phys. 79 (1983) 4279.
[6] M. Mayer, L.S. Cederbaum and H. Kppel, J. Chem. Phys. 100 (1994) 899.
[7] H.F. Davis, B. Kim, H.S. Johnston and Y.T. Lee, J. Phys. Chem. 97 (1993) 2172.
[8] K. Mikhaylichenko, C. Riehn, L. Valachovic and C. Wittig, unpublished.
[9] R.J. Yokelson, J.B. Burkholder, R.W. Fox, R.K. Talukdar and A.R. Ravishankara, J. Phys. Chem. 98 (1994) 13144.
[10] A.E. Douglas, J. Chem. Phys. 45 (1966) 1007.
[11] H.F. Davis, P.I. Ionov, S.I. Ionov and C. Wittig, Chem. Phys. Lett. 215 (1993) 214.
[12] H. Kppel, W. Domcke and L.S. Cederbaum, Adv. Chem. Phys. 57 (1984) 59.
[13] I.B. Bersuker and V.Z. Polinger, Vibronic interactions in molecules and crystals (Springer-Verlag, New York, 1989).
[14] D.W. Kohn, H. Clauberg and P. Chen, Rev. Sci. Instrum. 63 (1992) 4003.
[15] G. Schott and N. Davidson, J. Am. Chem. Soc. 80 (1958) 1841.
[16] H.S. Johnston and R.A. Graham, Can. J. Chem. 52 (1974) 1415.
[17] B. Kim, P.L. Hunter and H.S. Johnston, J. Chem. Phys. 96 (1991) 4057.
[18] R.E. Smalley, L. Wharton and D. H. Levy, J. Chem. Phys. 63 (1975) 4977.
[19] S.P. Sander, J. Phys. Chem. 90 (1986) 4135.
[20] A.R. Auty, in: The nitrate radical: physics, chemistry, and the atmosphere, Atmospheric Environment 25A, ed. R.P. Wayne (Pergamon Press, Oxford, 1991) p. 19.
[21] H.H. Nelson, L. Pasternack and J. R. McDonald, J. Phys. Chem. 87 (1983) 1286.
[22] T. Ishiwata, I. Fujiwara, Y. Naruge, K. Obi and I. Tanaka, J. Phys. Chem. 87 (1983) 1349.
[23] K. Kawaguchi, E. Hirota, T. Ishiwata and I. Tanaka, J. Chem. Phys. 93 (1990) 951.
[24] GAUSSIAN 92, Revision C, M.J. Frisch, G.W. Trucks, M. Head-Gordon, P.M.W. Gill, M.W. Wong, J.B. Foresman, B.G. Johnston, H.B. Schlegel, M.A. Robb, E.S. Replogle, R. Gomperts, J.L. Andres, K. Raghavachari, J.S. Binkley, C. Gonzalez, R.L. Martin, D.J. Fox, D.J. Defrees, J. Baker, J.J.P. Stewart and J.A. Pople (Gaussian, Inc., Pittsburgh, PA, 1992).
[25] M. Bixon and J. Jortner, J. Chem. Phys. 50 (1969) 4061.
[26] B.C. Garrett and D.C. Truhlar, J. Phys. Chem. 83 (1979) 2921.
[27] W.H. Miller, J. Am. Chem. Soc. 101 (1979) 6810.